Journal of Sol-Gel Science and Technology (2020) 96:226–235
https://doi.org/10.1007/s10971-020-05361-5

ORIGINAL PAPER: SOL–GEL AND HYBRID MATERIALS FOR CATALYTIC, PHOTOELECTROCHEMICAL AND SENSOR APPLICATIONS

Characteristics and photocatalytic activity of highly *c*-axis-oriented ZnO thin films

Didik Aryanto[1] · Erna Hastuti[2] · Melda Taspika[1] · Khoirul Anam[2] · Isnaeni Isnaeni[1] · Wahyu B. Widayatno[1] · Agus S. Wismogroho[1] · Putut Marwoto[3] · Bebeh W. Nuryadin[4] · Alfian Noviyanto[5,6] · Sugianto Sugianto[3]

Received: 17 May 2020 / Accepted: 30 June 2020 / Published online: 12 July 2020

Abstract

ZnO thin films are deposited on glass substrate using sol–gel spin coating methods with various annealing temperatures. The structural, morphological, and optical properties are studied by XRD, FE-SEM, UV–Vis, and photoluminescence spectrophotometer. The photocatalytic activity was assessed by examining the decomposition of Rhodamine-B (Rh-B) dye under UV illumination. The result shows that the ZnO films have a hexagonal wurtzite structure with highly preferred *c*-axis orientation. The (101) crystallographic plane appears at higher annealing temperatures. The transmittance of ZnO films is more than 80%, with a slight red shift in absorption and decrease in the optical band gaps as the annealing temperature increases to some extent. The photoluminescence spectra of the ZnO films at room temperature demonstrated the ultra-violet (UV) emission with a peak emission at 410 nm (3.03 eV). According to the photocatalytic activity examination, the presence of (101) plane in the *c*-axis oriented ZnO films enhances the photocatalytic performance by a factor of 5. The result revealed that ZnO films with multi-orientation structure possess better photocatalytic performance than that of the single-orientation ones. In particular, the photocatalytic performance is highly contributed by the polar crystal plane and slightly improved by the crystallinity and surface morphology.

✉ Didik Aryanto
didik_phys@yahoo.co.id

[1] Research Center for Physics, Indonesian Institute of Sciences, Kawasan Puspitek Serpong, Gd. 440-442, Tangerang Selatan, Banten 15314, Indonesia

[2] Department of Physics, Faculty of Science and Technology, UIN Maulana Malik Ibrahim, Jl Gajayana No. 50, Malang 65144, Indonesia

[3] Department of Physics, Universitas Negeri Semarang, Sekaran-Gunungpati, Semarang 50229, Indonesia

[4] Department of Physics, Universitas Islam Negeri Sunan Gunung Jati Bandung, Jl. A. H. Nasution 105, Bandung 40614, Indonesia

[5] Nano Center Indonesia, Jl. Puspiptek, Tangerang Selatan, Banten 15314, Indonesia

[6] Department of Mechanical Engineering, Mercubuana University, Jl. Meruya Selatan, Kebun Jeruk, Jakarta 11650, Indonesia

Graphical Abstract

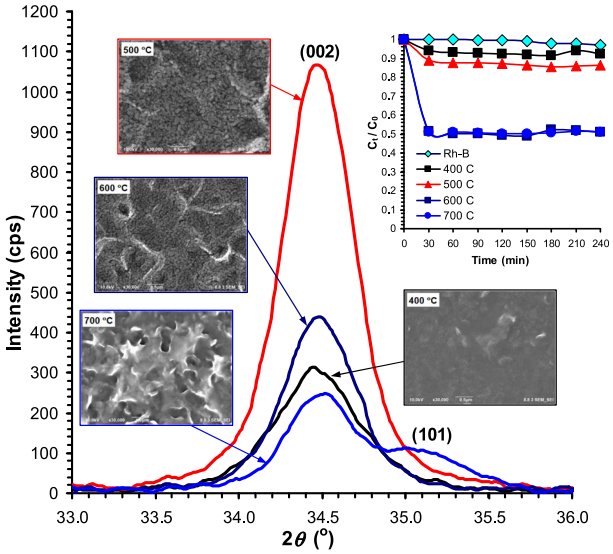

Keywords ZnO thin film · Photocatalysis · *c*-axis orientation · Photocatalytic activity

Highlights

- ZnO films with highly preferred *c*-axis orientation were prepared using sol–gel spin coating technique.
- The ZnO films have a transmittance more than 80% with an ultra-violet (UV) emission peak at 3.03 eV.
- The polar crystal plane gives more significant contribution on the photocatalytic performance than that of the crystallinity and surface morphology.

1 Introduction

ZnO is a II–VI semiconductor compound that has direct wide bandgap, similar with TiO_2 [1]. This compound has been widely used for many applications owing to its large exciton binding energy, relatively low cost, nontoxic nature [2, 3], and its high potential for degrading recalcitrant organic compound in wastewaters. Many studies on ZnO photocataysts show that their photocatalytic properties are highly related to the shape, size, surface morphology, and structure [4, 5]. The development of porous ZnO nanoparticles or nanostructures has been directed to increase their photocatalysis performance [4, 6]. However, powder-based photocatalysis have some drawbacks in water and air treatment applications, i.e, potential health and environmental risks due to their low separability, recoverability, as well as recyclability [3, 5]. In order to solve these problems, the utilization of ZnO compound as thin films for photocatalysis applications is highly preferable.

Various methods to fabricate ZnO thin films for photocatalysis applications such as aqueous chemical growth (ACG) [7], sol–gel [1, 3, 8–10], sputtering [5, 11], spray pyrolysis [12], atomic layer deposition [13], and electrodeposition [14] have been developed. Almost all studies show that ZnO thin film exhibits the photocatalytic activity in the range of 40–80%. The photocatalysis performance of the thin film is strongly influenced by structure, morphology, thickness, bandgap, and doping. Cataño et al. [14] showed that the photocatalytic activity of (0002) polar planes are greater than that of nonpolar perpendicular planes. Meanwhile, Ahumada-Lazo et al. [5] showed that the presence of (100) and (101) crystallographic planes in ZnO thin films significantly contributed to the improvement of photocatalytic activity. It has been also indicated that the crystallographic plane has a role in the photocatalytic performance [15]. However, there are limited reports that focus on studying the properties of (002) crystalligraphic plane in the photocatalysis applications.

In the present study, ZnO thin films have been fabricated by sol–gel spin coating method. The sol–gel preparation and parameters of this research are different with previous report by Natsume and Sakata [16], Kamaruddin et al. [17], and Gadallah and El-Nahass [18], especially in the solvent, stabilizer, films fabrication, and annealing treatment. Besides that, their works mainly focus on the structural and optical properties of the ZnO thin films prepared by sol–gel

methods. According to the previous works, we report the correlation of microstructures with the optical properties, as well as with their photocatalytic activities of *c*-axis oriented ZnO thin films.

2 Experimental

ZnO thin films were prepared according to our previous report [3]. In detail, ZnO solution was prepared by mixing zinc acetate dehydrate ($Zn(CH_3COO)_2{\cdot}2H_2O$), isopropanol ($C_3H_8O$), and ethanolamine ($C_2H_7NO$) as a precursor, solvent, and stabilizer, respectively. The molar ratio of isopropanol and zinc acetate dehydrate was 1.0. The mixed solution was stirred at 60 °C for 90 min. The as-prepared solution was then aged for 24 h at room temperature. While waiting for the aging process, a corning glass substrate was washed in an ultrasonic bath by acetone, methanol, and deionized water respectively, followed by drying at room temperature. Then, the aged ZnO solution was dropped onto the rotated corning glass (the rotation of corning glass was facilitated using VTC-100 spin coater system for 15 s at 2500 rpm). After that, the as-prepared ZnO films were preheated at 300 °C for 30 min to remove the solvent. Finally, the as-produced films were annealed in the air at various temperatures (400, 500, 600, and 700 °C) for 1 h.

The XRD patterns of ZnO films were recorded using Smartlab Rigaku X-ray diffractometer with the wavelength of 1.5418 Å. The morphological analysis was carried out using field emission scanning electron microscope (FE-SEM) JEOL JIB 4610F to observe the effect of heating on the surface of the samples. The ultra-violet (UV)–visible transmittance spectra were collected using HITACHI UH5300 spectrometer to observe the transparency of the films. The photoluminescence (PL) properties were studied using a femtosecond laser PL spectrometer (325 nm, 100 μJ). The photocatalytic activity of ZnO films were determined by evaluating the degradation of Rhodamine-B (Rh-B) solution under UV-light irradiation. In detail, the experiment was carried out at room temperature using Royalux T5 6 W lamps as UV source. The as-prepared films were immersed in 100 mL of a 10 ppm Rh-B solution and was irradiated by eight UV lamps. The absorbance intensity of Rh-B solution was measured for every 30 min using visible spectrophotometer AMTAST AMV01 to calculate degradation efficiency of Rh-B using the equation [19]:

$$\text{Degradation}(\%) = (C_0 - C_t)/C_0 \times 100 = (A_0 - A_t)/A_0 \times 100, \quad (1)$$

where C_0, C_t, A_0, and A_t is attributed to the initial concentration, the concentration after t min reaction, the initial absorbance, and the absorbance after t min reaction of the Rh-B the characteristic absorption wavelength of 550 nm, respectively.

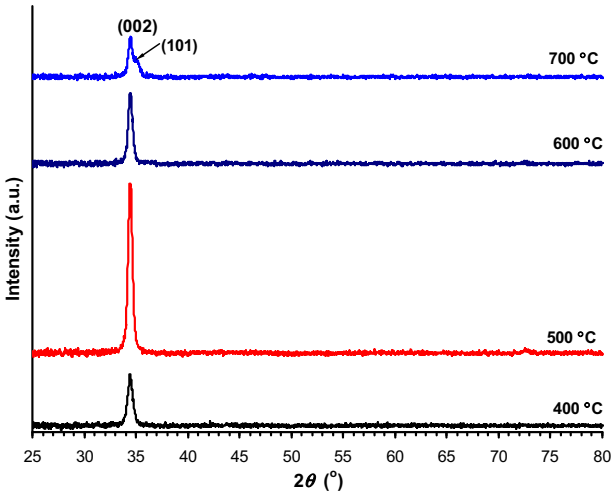

Fig. 1 XRD patterns of ZnO thin films showing the effect of annealing temperature

3 Results and discussion

3.1 Structure and morphology of ZnO thin films

The XRD patterns of ZnO thin films annealed at various temperatures are shown in Fig. 1. The samples exhibit the same strong peak located at $2\theta = 34.43°$, corresponding to the ZnO (002) plane (PDF Card No. 00-005-0664), regardless of different annealing temperature (shown in Fig. 2). There are no other peaks in the samples annealed at 400, 500, and 600 °C, which indicates a highly preferred *c*-axis orientation with a wurtzite structure has been formed [20]. The *c*-axis orientation, especially (002) plane, may be a common phenomenon in the ZnO film deposition by the chemical process using organo-zinc compounds [16]. The minimization of the surface energy and the internal stress is believed to be the reason for the preferential orientation [21]. In Fig. 2, the XRD peak intensity of sample at 500 °C is much higher than those at other temperatures. Improving the crystal quality of the ZnO films contributes to the increasing peak intensity [21]. As the annealing temperature was increased up to 600 °C, the peak intensity increases to some extent, which is likely due to the increasing grain size of the ZnO film. Interestingly, when the annealing temperature was increased further to 700 °C, the (002) peak intensity decreases and the small peak, relates to the (101) plane, presents at $2\theta = 35.12°$. These phenomena may be attributed to the insufficient supply of thermal energy for recrystallization, grain growth and powder nature of the films [22].

The average crystallite size of the films is calculated using Debye–Scherrer formula in Eq. (2) for (002) peak and is listed in Table 1 [23]:

$$D = \frac{0.9\,\lambda}{\beta\,\cos\theta}, \tag{2}$$

where λ, β, and θ is the utilized X-ray wavelength, full width at half maximum (FWHM) and Bragg diffraction of the (002) peak, respectively. It can be seen in Table 1 that the crystallite size of ZnO films increases from 14.15 to 19.82 nm as the annealing temperature increases to some extent. During annealing, the defects have tendency to merge, forming larger grains. Herein, the smaller FWHM value and larger crystallite size imply better crystallization. During annealing treatment, the nucleation of small grain into the larger one occurs when the energy is enough to facilitate the diffusion and recrystallization of the element or compound. The crystallite size of ZnO film annealed at 600 °C is smaller than that of the ZnO film annealed at 500 °C, which is likely due to the incomplete recrystallization at 600 C. This phenomenon also occurs owing to the formation or crystallization of new phase with a small grain size during annealing. As can be seen in Fig. 2, the peak pattern of the ZnO film annealed at 600 C is not balance, which indicates the incomplete formation of new phase.

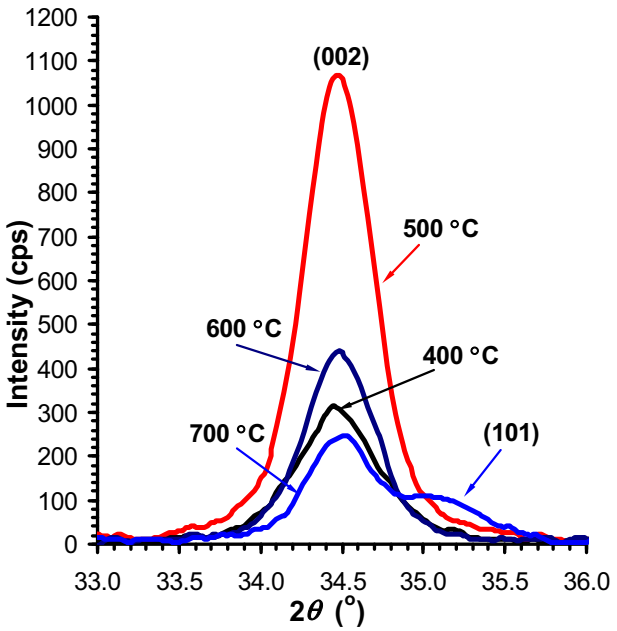

Fig. 2 The predominant orientations peak obtained from XRD of ZnO thin films as effect of annealing

The distribution of lattice constants, arising from crystal imperfections of the films, can be known from the lattice strain (ε), which was calculated using the tangent formula [23]:

$$\varepsilon = \frac{\beta}{(4\,\tan\theta)}. \tag{3}$$

Lattice strain is the influence on the length of dislocation lines per unit volume of the crystals. The dislocation density (ρ) can be expressed as [23]:

$$\rho = \left[\frac{\sqrt{12}\,\varepsilon}{D\,d}\right]. \tag{4}$$

The calculated lattice strain and dislocation density are included in Table 1. The decrease of lattice strain and dislocation density with respect to the annealing temperature indicates the decrease of the crystal imperfections. These lattice strains correspond to the stress of ZnO film, where it can be calculated using the following equation [24]:

$$\sigma = -233\,\text{GPa} \times \varepsilon. \tag{5}$$

The calculated stresses of ZnO film are shown in Table 1. All ZnO films have negative stress values, corresponding to the compressive stress. The lattice constant c of the annealed samples are higher than that of the pristine ZnO [25], which can be seen from the calculation results in Table 1 (based on PDF Card No. 00-005-0664, the lattice constant c of ZnO is 5.205 Å).

The strain and stress in the ZnO film is likely to present due to the extrinsic and intrinsic stresses. Herein, the lattice and the coefficient of thermal expansion mismatch between the glass substrate and ZnO film have significant contribution to the film stress. In addition, the lattice defects and impurities generated during the films synthesis can induce the film stress as well. This deduction is similar to the previous report by Mahmood et al. [25], Hasabeldaim et al. [26], and Chaitra et al. [21].

Figure 3 shows cross-sectional SEM images of the ZnO films annealed at 600 °C. Herein, the ZnO films have good

Table 1 List of parameters of ZnO thin films annealed at various temperatures which is calculated using (002) peak position

Annealing temperature (°C)	β	D (nm)	ε (%)	ρ ($\times 10^{-4}$) (line/nm^2)	σ (GPa)	c [Å]
400	0.588	14.15	0.475	0.45	−110.58	5.211
500	0.477	17.44	0.385	0.29	−89.68	5.210
600	0.488	17.06	0.394	0.31	−91.74	5.210
700	0.420	19.82	0.338	0.23	−78.79	5.199

adhesion to the substrate with the average thickness of 0.25 µm. Figure 4 shows FE-SEM images of ZnO thin films, annealed at different temperatures. It can be clearly seen that the microstructures of the ZnO thin films vary slightly depending the annealing temperature. The microstructure of the film annealed at 400 °C consists of larger island and smaller round-shaped particles within some clusters. In contrast, the film annealed at 500 °C exhibits nonuniform grains in the range of nano to micron size. By increasing the annealing temperature to 600 °C, the uniform finer grains can be obtained, which is in agreement with the XRD results. Herein, the progression of chemical reaction at higher temperature contributes to the enhanced uniformity of the film. As the result, the films become denser, while the growth rate is highly limited [27]. In addition, the good uniformity and homogeneity (Fig. 3b, c) of ZnO grain is likely due to the high degree of Zn–O domains mixing at the molecular level in a gel network during sol–gel synthesis. The Zn^{2+} ions will react with the O^{2-} ions to form ZnO particles. The phenomenon is also shown in the synthesis of Fe_2SiO_4–SiO and Fe_2O_3–SiO composite using sol–gel and solid state reaction [28]. Further increase to 700 °C induces the formation of agglomerated and compacted sheet with uneven pore distribution. These results indicate that higher annealing temperature leads to the increase of diffusion energy. The higher particles diffusion energy and films-substrate strain energy are likely contributed to the sheet formation on the substrate surface. Neighboring particles agglomerate to form sheets, where the incomplete process leads to the imperfect agglomeration at

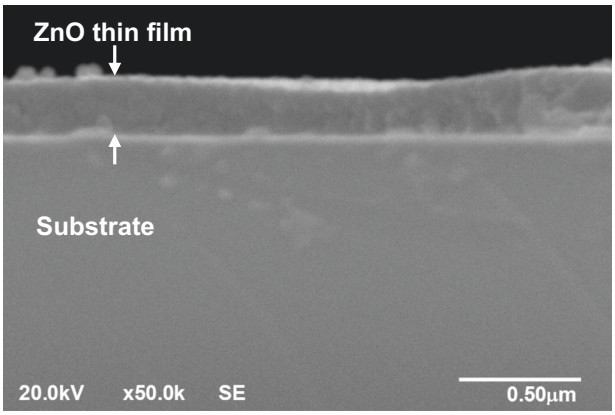

Fig. 3 Cross-sectional FE-SEM images of the ZnO films annealed at 600 °C

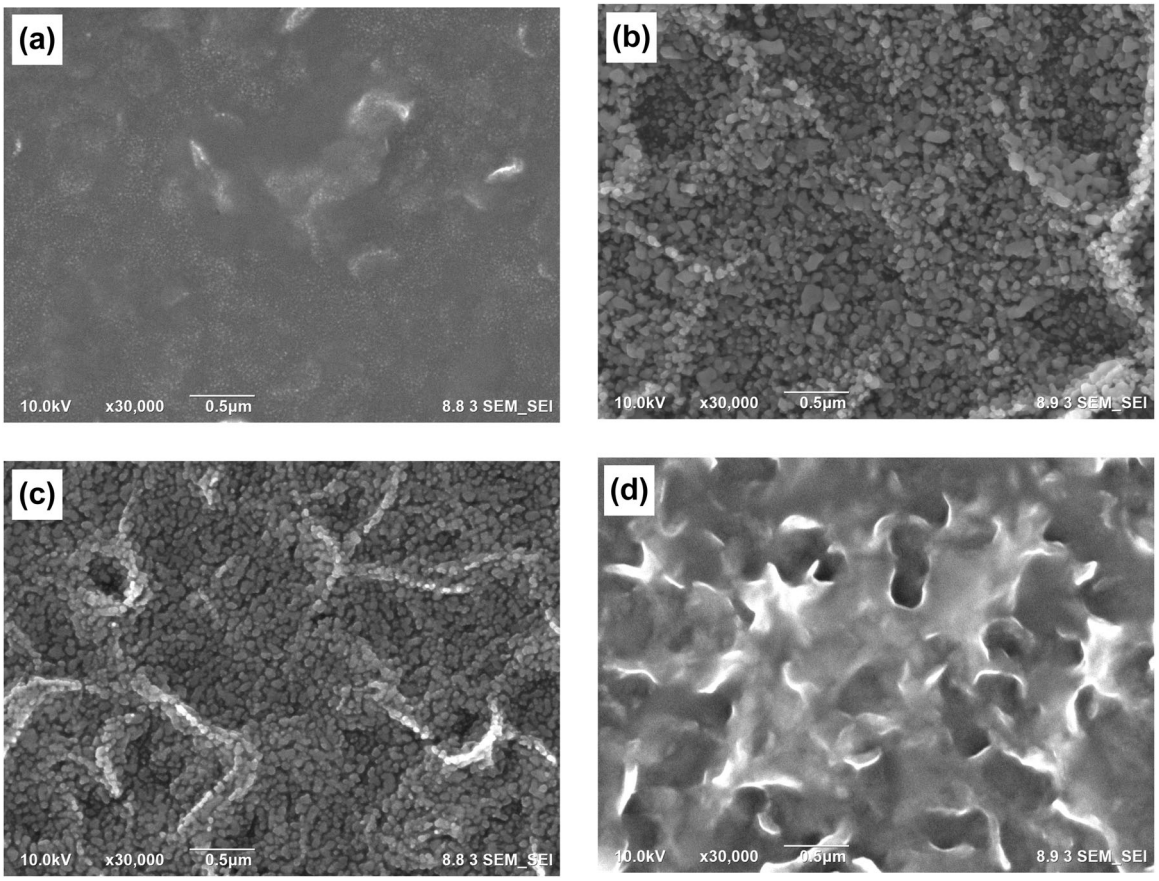

Fig. 4 FE-SEM images of ZnO thin films annealed at **a** 400 °C, **b** 500 °C, **c** 600 °C, and **d** 700 °C

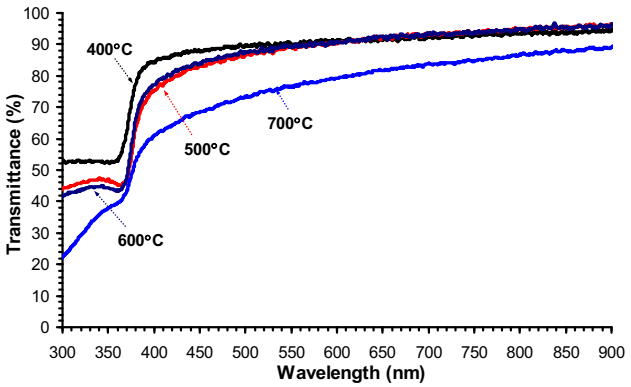

Fig. 5 Transmittance spectra of ZnO thin films as effect of annealing temperatures

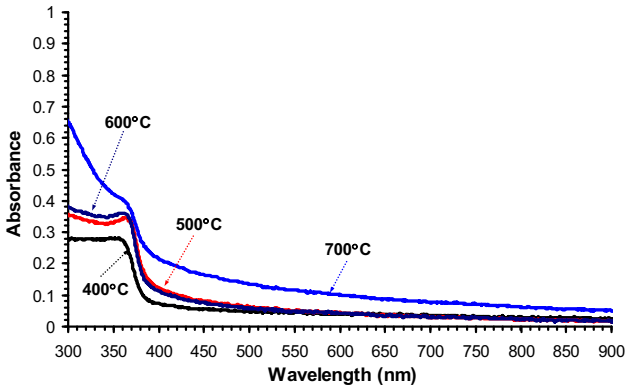

Fig. 6 Absorbance spectra of ZnO thin films as effect of annealing temperatures

the outer side of the grain and the formation of sharp edges on the sheets. The observed morphology evolution of ZnO thin film is also in a good agreement with the XRD data.

3.2 Optical properties of ZnO thin films

The transmittance spectra of ZnO thin films annealed at various temperatures in the wavelength range of 300–900 nm are shown in Fig. 5. All films exhibit high average transmittance, with more than 80% in the entire range of 420–900 nm and the fundamental absorption region before 380 nm wavelengths. However, the transmittance decreases as the annealing temperature increases to 700 °C. This phenomenon is highly possible due to the scattering effect from the rough surfaces [29]. The transmittance spectra of the ZnO films annealed at 500 and 600 °C show high similarity. These results are also in agreement with the FE-SEM and XRD results. It indicates that the optical properties of ZnO thin films depend on the structural homogeneity, crystallinity, and surface morphology.

Modification of the energy band structure of ZnO films for various annealing temperature can be found by using

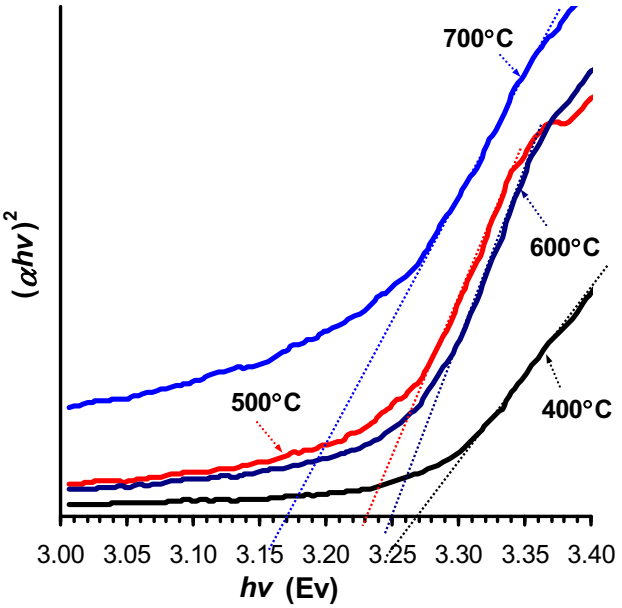

Fig. 7 Evolution of $(ahv)2$ vs. hv curves of ZnO thin films as effect of annealing temperatures

absorbance spectra. Figure 6 shows the absorbance spectra of ZnO thin films as an effect of annealing temperature in the wavelength region of 300–900 nm. The optical absorbance spectra of films are calculated using Beer' law with the following equation [20]:

$$A = 2 - \log(\%T), \tag{6}$$

where T is the transmittance and A is absorbance. At 400 °C, the fundamental absorption edge of ZnO films can be seen at 360 nm and clearly shifts to the red region as the annealing temperature increases. The slight modification of the band structure in the ZnO films can be attributed to the change of annealing temperature.

The optical band gaps (E_g) of the films can be estimated using the following relation [30]:

$$(\alpha hv)^n = B(hv - E_g), \tag{7}$$

where α is the absorption coefficient, B is a constant, hv is the discrete photon energy, and $n = 2$ (for direct bandgap semiconductors). The absorption coefficient α of the films is calculated from the transmittance using formula [31]:

$$\alpha = \frac{1}{t}\ln(1/T), \tag{8}$$

where t is thickness of the films. The energy gaps were estimated using extrapolation from the graph of $(\alpha hv)^2$ versus (hv) relationship. As shown in the Fig. 7, the optical band gaps decreases as the annealing temperature increases. The result shows the structural change, which is also in agreement with the XRD data in Fig. 1. Considering the

data in Table 1, the annealing treatment removes the defect, improves crystal quality, and changes the intrinsic stress of the films. Lee et al. [32] report that removal of oxygen vacancies in the films at higher annealing temperature might contributes to the decrease of bandgap energy. Previous studies show that the bandgap of ZnO thin films decreases as the grain size increases, which can be attributed to the effect of annealing temperature [8, 25]. In this work, the decrease of the band gaps is likely due to the increase of the grain size, which is correlated with the annealing temperature. It is corroborated by the FE-SEM result in Fig. 4, in which the grain size of the films increases linearly with the increasing annealing temperature.

The grain size of the films is strongly correlated with the intrinsic stress, which can be expressed as [25, 33]:

$$\sigma = \frac{E_f\,\delta}{\left(1-v_f\right)G}, \tag{9}$$

where E_f is Young's modulus, v_f is Poisson's ratio, δ is the interaction potential across the grain, and G is the grain size of the films. Equation (8) clearly shows that the intrinsic stress decreases as the grain size increases. The deduction is supported by the XRD and FE-SEM results, in which increasing annealing temperature stimulates the decrease of compressive stress and the increase of grain size. This phenomenon can be attributed to the increase of defect movement, which gives enough energy for atom rearrangement at higher annealing temperature.

Figure 8 shows the room temperature PL spectra of ZnO thin films at different annealing temperature, which confirms the XRD and FE-SEM results. The excitation wavelength of 325 nm is used in this experiment. All of ZnO thin films have a broad emission spectra, with the center of the peak around 410 nm (3.03 eV), which is associated to the UV emission. The broad UV emission on PL spectra is likely due to the poor quality of ZnO films and wider grain size distribution [34]. The UV emission is also attributed to the band-to-band excitonic recombination, which is highly related to the near-band-edge emission of ZnO [35, 36]. Previous works reported that the UV emission band is formed due to the most preferred orientation (002) of the ZnO [37], which is in agreement with the results of this work. The violet emission at 410 nm can also be attributed to the zinc interstition, which is also reported by Pathak et al. [38]. The weak and broad bands can also be observed at 750 nm (1.6 eV) when the annealing temperature is 500 °C. Wu et al. [39] and Kumar et al. [40] suggested that the visible emission peaks, centered at ~600–760 nm, is generally attributed to the higher defects such as vacancies and oxygen interstition. The sample annealed at 500 °C possesses the highest UV emission peak than that of the other samples, which may contribute to the improvement of the film crystallinity [41]. Another work by Chithira and John [42] also reported the increase of the grain size as the UV emission peak increases to some extent. It should be noted that the decreasing trend of UV emission peak for the samples annealed at 600 and 700 °C is likely due to the decrease of packing density of the film [40]. Furthermore, the coalescence of small crystals caused the displacement of grain boundaries at 600 and 700 °C, leading to the formation of non-radiative recombination centers [43].

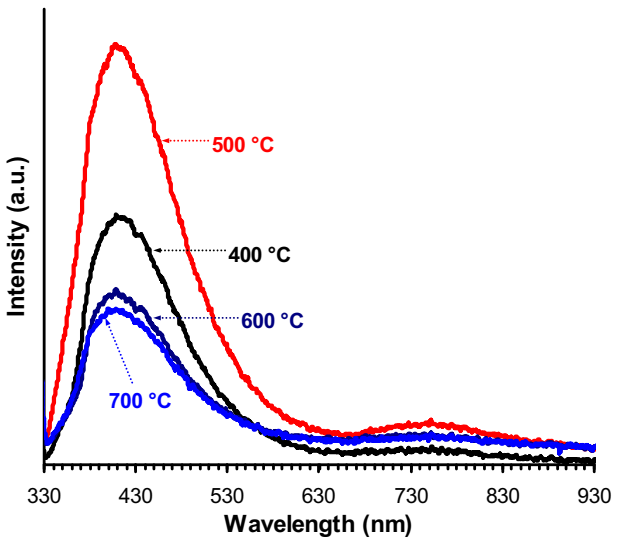

Fig. 8 Photoluminescence spectra of ZnO thin films annealed at various temperatures

3.3 Photocatalytic activity of ZnO thin films

The photocatalytic activity evaluation of ZnO thin films was conducted by measuring the photo-induced decolorization of Rh-B dye under UV-light irradiation. The experimental results for the Rh-B degradation (C_t/C_0) versus time are

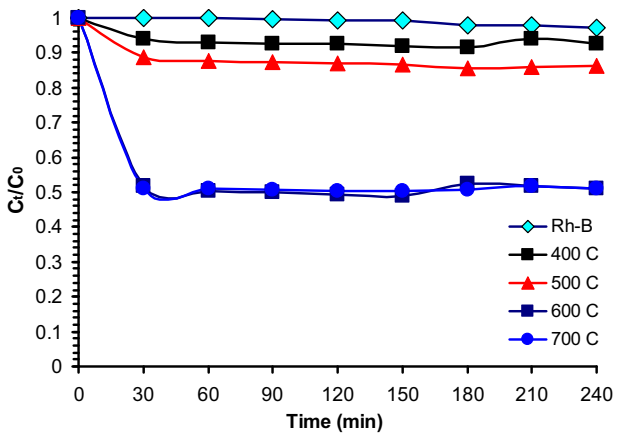

Fig. 9 Photodegradation curves of rhodamine-B using ZnO thin films as photocatalysis

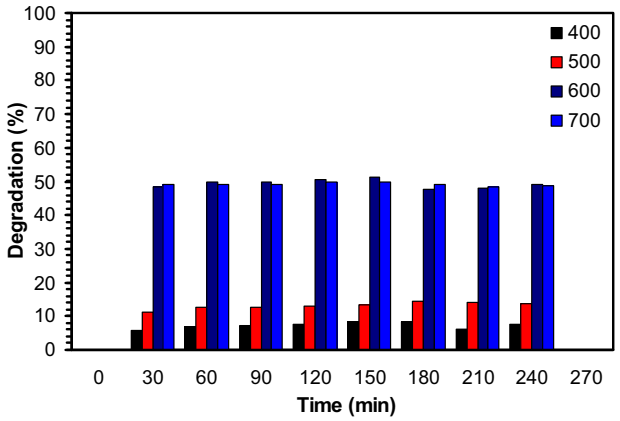

Fig. 10 Photocatalytic degradation of rhodamine-B under UV irradiation for 240 min

displayed in Fig. 9. The result shows that the photolysis by UV light without catalyst could not degrade Rh-B due to the absence of UV absorbing material that stimulates the photocatalytic activity [44]. Referring to the concept of ZnO photocatalysis in previous reports [8, 45], the UV-light irradiation will excite the electron from the valence band into the conduction band, leaving holes in the valence band. Briefly, at the conduction band, the oxygen acceptors will be reduced to form superoxide radical anion which will produce hydroxyl radicals. On the other hand, holes in the valence band will react with the absorbed water, producing the highly reactive hydroxyl radicals. Then, the resulted radicals will directly oxidize the organic pollutants and powerfully degrade the Rh-B. The contaminant molecules (i.e., Rh-B) will be absorbed onto the surface of ZnO thin films.

Figure 10 shows the photocatalytic degradation of Rh-B solution using ZnO thin film as a photocatalyst under UV irradiation for 240 min. The presence of ZnO films in the Rh-B dye stimulates the degradation of the dye, which was occurred after 30 min UV irradiation. The ZnO films annealed at 600 and 700 °C posses better photocatalytic performance than that of the samples annealed at 400 and 500 °C. All of the samples demonstrate complete and fast dye degradation after UV irradiation for 30 min. Herein, the different Rh-B degradation rate of around 7% and 13% is obtained when using ZnO films annealed at 400 and 500 °C, respectively. Nevertheless, similar performance (i.e., Rh-B dye degradation rate of 50%) is demonstrated when using ZnO films annealed at 600 and 700 °C. The result indicates that the photocatalytic performance of ZnO films can be increased by increasing annealing temperature during ZnO films fabrication. It should be noted from the results that photocatalytic activity is enhanced as the annealing temperature is increased to some extent, which is likely due to the increase of ZnO film grain size as has been also reported by the previous reports [8]. Considering the XRD results of ZnO films annealed at 500 and 600 °C (Fig. 1), the decrease of photocatalytic activity performance could be explained by the increased possibility of the formation of structural defect [46]. This argumentation is also supported by the PL results (Fig. 8), which is shown by the presence of visible emission peaks as an indication of the existence of structural defect within the films. Herein, the trend of photocatalytic performance of the films could be explained by the condition of polar crystal plane. From the photocatalytic test results, it can be seen that the presence of (101) plane improves the photocatalytic performance. At annealing temperature of 600 °C, the growth transition of (101) plane is likely to occur within the crystal structure beside (002) plane, which is indicated by the decrease of peaks intensity and the broadening FWHM (Fig. 2). Since the (101) reflection is positively charged, OH^- ion would be preferentially adsorbed, leading to a greater production of OH• radicals [15], which ease the generation of H_2O_2 [5]. Thus, the presence of (101) plane is likely to have significant contribution to the photocatatlytic activity. According to this works, the influence of (101) plane in the photocatalytic performance is more dominant than that of the crystal parameters and surface morphology. The photocatalytic performance increases by a factor of 5 when (101) plane is grown on the ZnO films. This confirms that the photocatalytic performance of the ZnO films with multi-orientation is better than that of the single-orientation ones.

4 Conclusions

ZnO thin films were prepared on glass substrate using sol–gel spin coating technique. The effect of various annealing temperature on the microstructure, optical properties, and photocatalytic activity of ZnO thin films was investigated. The ZnO films have a hexagonal wurtzite structure with highly preferred *c*-axis orientation, which is indicated by the presence of single peak at (002) plane. At higher temperature, ZnO films become multi-orientation with the occurence of (101) crystallographic plane. Different annealing temperature gives different ZnO films morphology. The average transmission of all ZnO films is >80% in the wavelength range of 420–900 nm. The bandgap energy of ZnO films decreases as the annealing temperature increases. The complete and fast degradation of the Rh-B dye occurs after UV irradiation for 30 min. The photocatalytic performance of ZnO films can be increased by the presence of (101) plane at higher annealing temperature. It can be concluded that the photocatalytic performance of multi-orientation ZnO films is better than that of the single-orientation ones.

Acknowledgements This research was supported by Ministry of Research, Technology and Higher Education, Indonesia under Grant No. 013/P/RPL-LIPI/INSINAS-2/VII/2018. The authors acknowledge Research Center for Physics-LIPI for providing the research facilities.

Compliance with ethical standards

Conflict of interest The authors declare that they have no conflict of interest.

Publisher's note Springer Nature remains neutral with regard to jurisdictional claims in published maps and institutional affiliations.

References

1. Talebian N, Nilforoushan MR, Ghasem RR (2012) Enhanced photocatalytic activities of ZnO thin films: a comparative study of hybrid semiconductor nanomaterials. J Sol-Gel Sci Technol 64:36–46
2. Wanotayan T, Panpranot J, Qin J, Boonyongmaneerat Y (2018) Microstructures and photocatalytic properties of ZnO films fabricated by Zn electrodeposition and heat treatment. Mater Sci Semicond Process 74:232–237
3. Aryanto D, Hastuti E, Husniya N, Sudiro T, Nuryadin BW (2018) Synthesis, characterization, and photocatalytic properties of nanocrystalline NZO thin films. J Phys Conf Ser 985:012025. (1-6)
4. Mclaren A, Solis TV, Li G, Tsang SC (2009) Shape and size effects of ZnO nanocrystals on photocatalytic activity. J Am Chem Soc 131:12540–12541
5. Ahumada-lazo R, Torres-Martinez LM, Ruiz-Gomez MA, Vega-Becerrra OE, Figueroa-Torres MZ (2014) Photocatalytic efficiency of reusable ZnO thin films deposited by sputtering technique. Appl Surf Sci 322:35–40
6. Cong W, Lin C (2011) Preparation, spectral characteristics and photocatalytic activity of Eu^{3+}-doped WO_3 nanoparticles. J Rare Earths 29:727–731
7. Chang Y-C, Chen C-M, Guo JY (2018) Fabrication of novel ZnO nanoporous films for efficient photocatalytic applications. J Photochem Photobiol A Chem 356:340–346
8. Lv J, Gong W, Huang K, Zhu J, Meng F, Song X, Sun Z (2011) Effect of annealing temperature on photocatalytic activity of ZnO thin films prepared by sol–gel method. Superlattices Microstruct 50:98–106
9. Jongnavakit P, Amornpitoksuk P, Suwanboon S, Ratana T (2012) Surface and photocatalytic properties of ZnO thin film prepared by sol–gel method. Thin Solid Films 520:5561–5567
10. Zheng G, Shang W, Xu L, Guo S, Zhou Z (2015) Enhanced photocatalytic activity of ZnO thinfilms deriving from a porous structure. Mater Lett 150:1–4
11. Cruz MRA, Ceballos-Sanchez O, Luévano-Hipólito E, Torres-Martínez LM (2018) ZnO thin films deposited by RF magnetron sputtering: Effect of the annealing and atmosphere conditions on the photocatalytic hydrogen production. Int J Hydrog Energy 43:10301–10310
12. Jayaraman VK, Hernández-Gordillo A, Bizarro M (2018) Importance of precursor type in fabricating ZnO thinfilms for photocatalytic applications. Mater Sci Semicond Process 75:36–42
13. Mauro AD, Fragalà ME, Privitera V, Impellizzeri G (2017) ZnO for application in photocatalysis: From thin films to nanostructures. Mater Sci Semicond Process 69:44–51
14. Cataño FA, Gomez H, Dalchiele EA, Marotti RE (2014) Morphological and structural control of electrodeposited ZnO thin films and its influence on the photocatalytic degradation of methyl orange dye. Int J Electrochem Sci 9:534–548
15. Jang ES, Won J-H, Hwang S-J, Choy J-H (2006) Fine tuning of the face orientation of ZnO crystals to optimize their photocatalytic activity. Adv Mater 18:3309–3312
16. Natsume Y, Sakata H (2000) Zinc oxide films prepared by sol-gel spin-coating. Thin Solid Films 372:30–36
17. Kamaruddin SA, Chan K-Y, Yow H-K, Sahdan MZ, Saim H, Knipp D (2011) Zinc oxide films prepared by sol–gel spin coating technique. Appl Phys A 104:263–268
18. Gadallah A-S, El-Nahass MM (2013) Structural, Optical constants and photoluminescence of ZnO thin films grown by sol-gel spin coating, Advances in. Condens Matter Phys 2013:1–11
19. Meng F, Song X, Sun Z (2009) Photocatalytic activity of TiO_2 thin films deposited by RF magnetron sputtering. Vacuum 83(9):1147–1151
20. Arif M, Sanger A, Vilarinho PM, Singh A (2018) Effect of annealing temperature on structural and optical properties of sol-gel-derived ZnO thin films. J Electron Mater 47:3678–3684
21. Chaitra U, Kekuda S, Rao KM (2017) Effect of annealing temperature on the evolution of structural, microstructural, and optical properties of spin coated ZnO thin films. Ceram Int 43:7115–7122
22. Hunge YM, Mahadik MA, Moholkar AV, Bhosale CH (2017) Photoelectrocatalytic degradation of phthalic acid using spray deposited stratified WO_3/ZnO thin film under sunlight illumination. Appl Surf Sci 420:764–772
23. Aryanto D, Jannah WN, Masturi, Sudiro T, Wismogroho AS, Sebayang P, Sugianto, Marwoto P (2017) Preparation and structural characterization of ZnO thin films by sol-gel method. J Phys Conf Ser 817:012025. (1–7)
24. Marwoto P, Wibowo E, Suprayogi D, Sulhadi, Aryanto D, Sugianto (2016) Properties of ZnO:Ga thin films deposited by dc magnetron sputtering: influence of Ga-doped concentrations on structural and optical properties. Am J Appl Sci 13:1394–1399
25. Mahmood A, Ahmed N, Raza Q, Khan TM, Mehmood M, Hassan MM, Mahmood N (2010) Effect of thermal annealing on the structural and optical properties of ZnO thin films deposited by the reactive e-beam evaporation technique. Phys Scr 82:065801. (1–8)
26. Hasabeldaim E, Ntwaeaborwa OM, Kroon RE, Coetsee E, Swart HC (2017) Effect of substrate temperature and post annealing temperature on ZnO:Zn PLD thin film properties. Opt Mater 74:139–149
27. Ilegbusi OJ, Khatami SMN, Trakhtenberg LI (2017) Spray pyrolysis deposition of single and mixed oxide thin films. Mater Sci Appl 8:153–169
28. Wang C, Shaw LL (2014) On synthesis of Fe_2SiO_4/SiO_2 and Fe_2O_3/SiO_2 composites through sol-gel and solid-state reactions. J Sol-Gel Sci Technol 72:602–614
29. Zhang XL, Hui KS, Bin F, Hui KN, Li L, Cho YR, Mane RS, Zhou W (2015) Effect of thermal annealing on the structural, electrical and optical properties of Al–Ni co-doped ZnO thin films prepared using a sol–gel method. Surf Coat Technol 261:149–155
30. Vajargah PH, Abdizadeh H, Ebrahimifard R, Golobostanfard MR (2013) Sol–gel derived ZnO thin films: Effect of amino-additives. Appl Surf Sci 285:732–743
31. Thirumoorthi M, Prakash JTJ (2015) Structural, morphological characteristics and optical properties of Y doped ZnO thin films by sol–gel spin coating method. Superlattices Microstruct 85:237–247
32. Lee S-M, Joo Y-H, Kim C-I (2014) Influences of film thickness and annealing temperature on properties of sol-gel derived ZnO-SnO_2 nanocomposite thin film. Appl Surf Sci 320:494–501
33. Tsai KY, Chin T-S, Shieh H-PD, Ma CH (2004) Effect of as-deposited residual stress on transition temperatures of VO_2 thin films. J Mater Res 19:2306–2314
34. Li BS, Liu YC, Zhi ZZ, Shen DZ, Lu YM, Zhang JY, Fan XW (2002) The photoluminescence of ZnO thin films grown on Si (100) substrate by plasma-enhanced chemical vapor deposition. J Cryst Growth 240(3–4):479–483
35. Do A-TT, Giang HT, Do TT, Pham NQ, Ho GT (2014) Effect of palladium on the optical and hydrogen sensing characteristics of Pd-doped ZnO nanoparticles. Beilstein J Nanotechnol 5:1261–1267

36. Dogar S, Kim SD (2016) Effects of high-temperature rapid thermal annealing for seed layers on the crystallographic evolution in hydrothermal ZnO nanostructures. Mater Sci Semicond Process 56:127–136
37. Kumar V, Swart HC, Ntwaeaborwa OM, Kroon RE, Terblans JJ, Shaat SKK, Yousif A, Duvenhage MM (2013) Origin of the red emission in zinc oxide nanophosphors. Mater Lett 101:57–60
38. Pathak TK, Kumar V, Swart HC, Purohit LP (2016) Electrical and optical properties of p-type codoped ZnO thin film prepared by spin coating technique. Phys E Low-Dimens Syst Nanostruct 77:1–6
39. Wu L, Wu Y, Pan X, Kong F (2006) Synthesis of ZnO nanorod and the annealing effect on its photoluminiscence property. Opt Mater 28:418–422
40. Kumar M, Dubey S, Rajendar V, Park S-H (2017) Fabrication of ZnO thin films by sol-gel spin coating and their UV and white-light emission properties. J Electron Mater 46(10):6029–6037
41. Goswami M, Adhikary NC, Bhattacharjee S (2018) Effect of annealing temperatures on the structural and optical properties of zinc oxide nanoparticles prepared by chemical precipitation method. Optik 158:1006–1015
42. Chithira PR, John TT (2017) The influence of vacuum and annealing on the visible luminescence in ZnO nanoparticles. J Lumin 185:212–218
43. Kuo S-Y, Chen W-C, Lai F-I, Cheng C-P, Kuo H-C, Wang S-C, Hsieh W-F (2006) Effects of doping concentration and annealing temperature on properties of highly-oriented Al-doped ZnO films. J Cryst Growth 287:78–84
44. Gao S, Zhang J, Li W, Jiao S, Nie Y, Fan H, Zeng Z, Yu Q, Wang J, Zhang X (2018) Near room temperature and large-area synthesis of ZnO/Cu_2O heterojunction for photocatalytic properties. Chem Phys Lett 692:14–18
45. Shahine I, Beydoun N, Gaumet JJ, Bendeif E-E, Rinnert H, Magri P, Naciri AE, Miska P, Jradi S, Akil S (2019) Pure, size tunable ZnO nanocrystals assembled into large area PMMA layer as efficient catalyst. Catalysts 9(2):162. (1–24)
46. Andrade JdL, Oliveira AG, Mariucci VVG, Bento AC, Companhoni MV, Nakamura CV, Lima SM, Andrade LHdC, Moraes JCG, Hechenleitner AAW, Pineda EAG, Fernandes DM (2017) Effects of Al^{3+} concentration on the optical, structural, photocatalytic and cytotoxic properties of Al-doped ZnO. J Alloy Compd 729:978–987